EFFECTS OF INJECTION SPEED ON MECHANICAL PROPERTIES IN HIGH-PRESSURE DIE CASTING OF MG-RE ALLOY

YUKI KASHIWABARA[1], MOHD DANIAL IBRAHIM[2], LIDYANA BINTI ROSLAN[2], HITOSHI WATANABE[3], YUTA SUNAMI[4]

[1]Graduate School of Science and Technology, Tokai University

[2]Department of Mechanical and Manufacturing Engineering, Faculty of Engineering, Universiti Malaysia

[3]Kyokuto Die-Casting Co, Japan

[4]Department of Mechanical Engineering, Tokai University, Japan

Best Student Paper Award of the 5th International Conference on Design Engineering and Science (ICDES 2020), Japan, November 4-5, 2020

DOI: 10.17973/MMSJ.2021_10_2021085

sunami@tokai-u.jp

In this study, in order to clarify the unknown physical properties of the Mg-Al-Th-RE alloy, the relationship between the injection conditions and the internal porosities and the mechanical properties exerted by the solidification microstructure were investigated. The obtained cast samples were investigated using X-ray CT internal measurements, tensile tests, Vickers hardness tests and solidification microstructure observations. The flow simulation and the X-ray CT analysis results showed that the porosity volume increased as the injection speed increases. The higher injection speed also affected the metal microstructure to become denser, which leads to a higher material strength and hardness. The eutectic phases quickly formed because of the shorter filled and cooled time. Therefore, the growth of the primary phase α-Mg was suppressed. On the other hand, it was considered that the material strength and hardness were greatly reduced by the coarse primary phase.

KEYWORDS

high-pressure die casting, magnesium alloy, simulation, x-ray computed tomography, tensile tests, Vickers hardness tests, microstructure

1 INTRODUCTION

In today's world, where global environmental issues are becoming increasingly important, regulations on carbon dioxide (CO_2) emissions are becoming stricter year by year. In particular, the improvement of fuel efficiency of automobiles, which account for the majority of CO_2 emissions, is eagerly desired from around the world. Among the measures to improve fuel efficiency, weight reduction of the vehicle body is simple and effective, and the conversion of materials from conventional iron parts is being promoted. Among them, magnesium (Mg) is expected to be popular because it has features such as higher specific strength and specific rigidity than iron and aluminum, rich resources, and recyclability. High-pressure die casting (HPDC) is a technology that is indispensable for the production of magnesium auto parts. HPDC is a casting method that injects molten metal into a mold at high speed and high pressure, thereby shortening the manufacturing cycle as much as possible. For this reason, die casting has been established as a system capable of mass-producing products with excellent casting surface in a short time. However, characteristic porosities such as porosity and inclusion of solidified fragments occur in die cast products. In particular, the cavities caused by air entrainment and solidification shrinkage causes not only deterioration of mechanical properties but also leakage of pressure-resistant members. Therefore, there is a need to elucidate the mechanism of porosity generation, and optimization of the injection speed have been performed with CFD [Kuriyama 2012, Cleary 2014, Ibrahim 2017, Roslan 2018, Niida 2020]. Research related to quantitative measurements are also being performed [Yanagihara 2015, Gaspar 2016, Rimar 2016, Gaspar 2019]. These studies have been actively conducted on aluminum alloys and zinc alloys. Although, research and developments on magnesium alloys have not progressed because of material features such as flammability and poor castability. Magnesium alloys are generally difficult to be casted because of the ignition and the low specific heat, easy solidification, and poor fluidity. Heat-resistant and flame-retardant magnesium alloys with improved properties have been actively used and have been applied to automotive parts as practical materials [Beals 2004, Moscovitch 2007, Ebel-Wolf 2008, Mizutani 2019, Fukatsu 2021]. Among them, Mg-Al-Th-RE alloy is a magnesium alloy with improved heat resistance by adding calcium (Ca) and rare-earth (RE) elements, and with excellent fluidity to which aluminum (Al) is added at about 8% or more. It is expected to be used for products with complicated shapes that makes it difficult to fill the molten metal uniformly.

However, Mg-Al-Th-RE alloy internal microstructures and mechanical properties have not been elucidated for those actually casted in die casting processes. Die-casting magnesium alloys generally have eutectic microstructures composed primary and eutectic phases crystallized from a liquid phase. According to Mondal et al., the microstructures of magnesium alloy MRI153M are primary phase α-Mg and eutectic $Mg_{17}Al_{12}$ and $(Mg, Al)_2Ca$ phases, and the amount of $(Mg, Al)_2Ca$ is related to creep behavior [Mondal 2010]. Sun et al. examined the effect of casting thickness on the tensile properties of AZ91 magnesium alloy. The high tensile properties were attributed the low porosity level, fine dendrite microstructure, high eutectic content, and thick skin due to decreasing the thickness [Sun 2020]. From these literatures, it shows that it is necessary to know the correlation between the solidification microstructure and the material strength and to find conditions that can maximize its physical properties.

Taking from some examples of previous researchers conducting modifications of dimension, geometries, and new texturing [Ibrahim 2018, Kikuchi 2019], in this study, the relationship between the injection conditions and the internal porosities, and the mechanical properties exerted by the solidification microstructure were investigated to clarify the unknown physical properties of the Mg-Al-Th-RE alloy. The obtained cast samples were investigated using X-ray CT internal measurements, tensile tests, Vickers hardness tests and solidification microstructure observations.

2 SIMULATION AND EXPERIMENTAL PROCESS

2.1 *Simulation method*

Tab. 1 shows the chemical composition of the Mg-Al-Th-RE alloy. The Mg-Al-Th-RE alloy is flame-retardant and is from the Mg-Al-Th-RE group. The heat resistance by Th and La of rare earths and the flame retardancy by Ca and Sr have been

improved. Fig. 1 shows the analysis model used in this paper. The model is called step-type test piece. The test piece face on moving die wall is called step side as shown in Fig. 1(a), and the test piece face on fixed die wall is called flat side. The cavity size is 200 mm in height, 100 mm in width and a staggered step consisting of 4, 8, 12, and 16 mm in its thickness as shown in Fig. 1(a) and 1(b). The thickness will help to explain casting properties followed general thickness of die casting products. The runner was a typical T-shape, and the overflow was set on the side of 12 mm and 16 mm parts, which were the final filled positions as shown in Fig. 1(c). The physical properties of the Mg-Al-Th-RE alloy were obtained by material properties calculation software JMatPro. This software calculates thermodynamic properties from a chemical composition of an alloy. The CALPHAD (Calculation of phase diagram) method is applied to the thermodynamic model and the Modified Scheil-Guliver model is applied to the solidification calculation. The mold filling process were simulated with the casting simulation software JSCAST. The basic equations were the continuity equation, the Navier-Stokes equation, and the energy equation. The simulation methods were three-dimensional numerical model of single-phase flow of liquid phase based on the direct finite difference method and the Volume of Fluid (VOF) method. Tab. 2 shows the simulation conditions. The thermophysical properties of the Mg-Al-Th-RE alloy determined by the JMatPro were set the material parameters. The die material used is the SKD61 die steel. This steel is the most widely used in die casting dies all over the world. The meshing properties were based on orthogonal elements of 1.0 mm

Al	Th	Ca	Sr	Ce	Mn	La	Pr
8.51	2.26	>0.42	0.22	0.14	0.11	0.079	0.045
Si	Y	Zn	P	Fe	Sn	Zr	Mg
0.027	0.020	0.0080	0.0027	0.0013	0.0014	0.0010	Bal.

Table 1. Chemical composition of Mg-Al-Th-RE alloy (mass%)

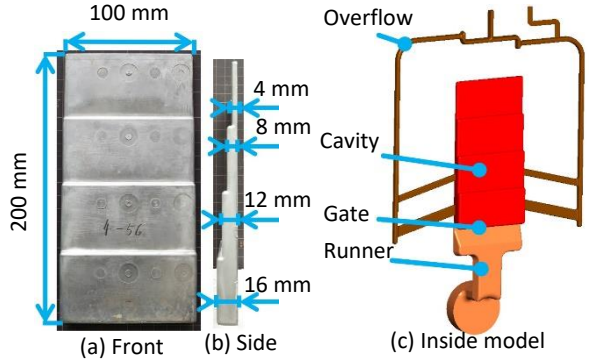

Figure 1. Schematic diagram of steps-type test piece

Fluid		Mg alloy
Mold		SKD61
Injection speed	First v_1 [m/s]	0.3
	Second v_2 [m/s]	2.0, 5.0
Casting pressure P [MPa]		70
Temperature T [K]		953
Kinematic viscosity υ [m^2/s]		1.0×10^{-6}
Critical pressure P_c [MPa]		20
Thickness of gate t_g [mm]		6.0
Mesh size x [mm]		1.0

Table 2. Simulation conditions

where Tetra-meshes were applied to the model surface. The injection conditions were the two-stage injection with the first injection speed v_1 of 0.3 m/s and second speed v_2 of 2.0 and 5.0 m/s. When the model is filled at 39.6%, the injection speed is switched with the high speed. The calculation was finished at the filling rate of 99%, and is considered as converged. Then, an injection pressure P is raised 70 MPa. The pouring temperature T was set at a constant value of 953 K and the kinematic viscosity υ was set to 1.0 × 10^{-6} m^2/s. The vent pressure was set as the atmospheric pressure, and the flow was stopped once the internal pressure of the air in the mold exceeded 20 MPa. The gate thickness t_g was set as 6.0 mm from the flat side as shown in Fig. 2. It was determined due to relatively easy cutting on actual casting.

2.2 *Experimental method*

The step-type test pieces were manufactured by HTPC using a 350-ton cold chamber die casting machine (Ds-350EX, Toyo Machinery & Metal Co., Ltd.). Fig. 3 shows a schematic diagram of a die casting system. Tab. 3 shows the casting conditions. The gate thickness was 6.0 mm. Magnesium alloys were easily solidified because of the low specific heat value compared to the aluminum alloys. Thus, the injection speed was higher than

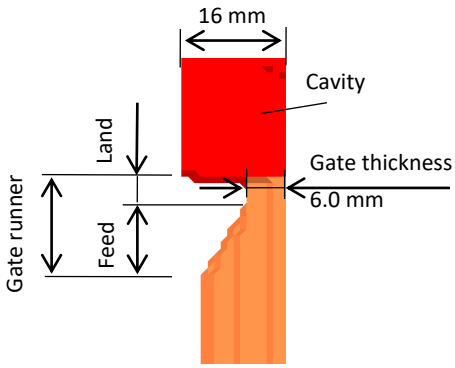

Figure 2. Gate runner model showing side view of casting

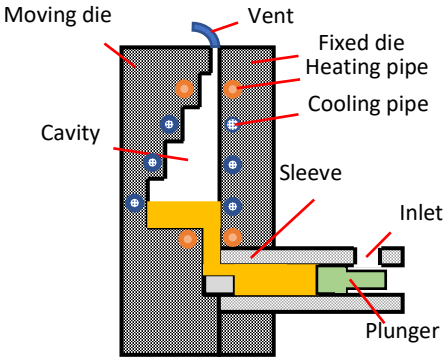

Figure 3. Schematic diagram of casting equipment

Method		HPDC
Machine		Ds350EX Toyo Machinery & Metal Co., Ltd.
Injection speed	First v_1 [m/s]	0.3
	Second v_2 [m/s]	2.0, 5.0
Casting pressure P_c [MPa]		70
Pouring temperature T_p [K]		953
Die temperature T_d [K]		423
Gate thickness t_g [mm]		6.0
Number N		10

Table 3. Casting conditions

the speed used in aluminum alloy die castings. The second injection speeds v_2 were set to 2.0 m/s and 5.0 m/s. Ten specimens were prepared under 2.0 m/s and 5.0 m/s conditions. The property measurements and the tensile tests were performed on four randomly selected samples were chosen.

X-ray CT (Nikon Instech, XTH225) was used for internal porosities measurement. The jig of sample stage made from a Styrene foam on an acrylic base plate is shown in Fig. 4. The jig was prepared to set specimens so that proper X-rays figures was able to be obtained. Styrene foam spacers used to simplify the analysis process were also inserted between the specimens. The X-ray CT conditions are shown in Tab. 4. During the measurements using the X-ray photography, the four test pieces were overlapped with angles in order to suppress the change in the transmittance. This is because a single test piece has a noticeable difference in the amount of transmission due to the variance between the width of 100 mm and the thickness of 4 to 16 mm, making it difficult to match the overall resolution. Based on the relationship between the detector size of 2000 pix × 2000 pix, the object to be photographed was regarded as a prism with a top surface of 100 mm × 100 mm including the spacer, and the magnification was determined to be 150 dpi. At this time of measurement, the minimum detectable porosity diameter was approximately about 0.3 mm. CT reconstruction was performed using CT Pro (Nikon). The metal hardening was applied to the photographed image because metal artifacts were noticeable. CT analysis software (Volume Graphics, VG Studio MAX 3.1) was used for porosity analysis. The boundary between the object and surrounding air was determined using the center gradation between the peaks of the color histogram of the reconstructed CT data. Fig. 5 shows the analysis method of X-ray CT. In the figure, the gray area shows the material, and the black area shows a void existing the air and a scale bar shows a length of 1.5 mm. Fig. 5(a) shows the void detected the area surrounded by sky blue using the standard algorithm of void analysis with VG Studio MAX. If the void detection is performed using the algorithm, the difficult void to confirm as a porosity is detected as shown in Fig. 5(a). In this paper, the void was detected the threshold analysis method. Fig. 5(b) shows the void detected the area surrounded by violet using the threshold analysis method. The threshold analysis method qualitatively detects the void using the threshold value of the gray scale to be regarded as a porosity as shown in Fig. 5 (b). This method is able to reduce a low accuracy void.

Fig. 6 shows the dimension of test specimen. The tensile test specimen was 20 mm wide, 4 mm thickness and 25 mm gage length. The test specimen was made using water jet cutting from 4 mm thickness of the test piece. Tensile tests were carried out with a 1 mm/min crosshead rate using a universal testing machine (Shimadzu Corporation, AG-100 kN X plus). The fractured specimens were measured by X-ray CT to determine the number of internal porosities. Four test pieces which has a thickness of 4mm were stacked, and only the parallel part with a width of 20 mm was measured. At this time, the minimum detectable void diameter is about 0.15 mm.

The hardness of the material was measured using a Vickers hardness tester (AVK-A, manufactured by Akashi Seisakusho). Nine measurement points were taken as shown in Fig. 6, and the average of the seven points excluding the maximum and minimum values was taken as the Vickers hardness. The rolling load is 5 kgf and the rolling time is 15 s. For the microstructure observation, the observation surface was sanded and buffed in

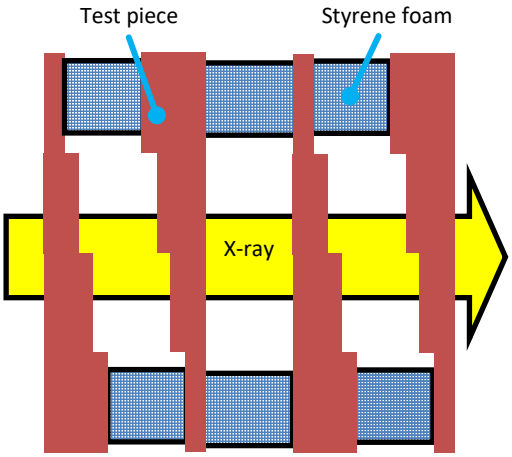

Figure 4. Overlapping tomography

X-ray CT equipment	XT H225 Nikon
CT analysis	VGSTUDIO MAX 3.1 Volume Graphics
Voltage *V* [kV]	225
Electric current *I* [μA]	220
Exposure time *t* [s]	1.42
Filter *f* [mm]	Cu 2.0
Resolution *I* [dpi]	150
Number of tomograms *n*	2000
Number of samples N_x	4
Penetrated thickness ratio	5:2

Table 4. X-ray CT conditions

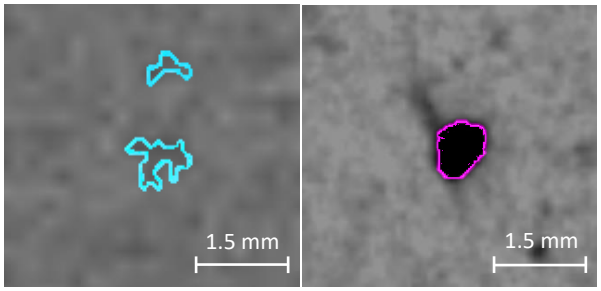

(a) Automatic analysis (b) Gray histogram analysis

Figure 5. Analysis method of X-ray CT

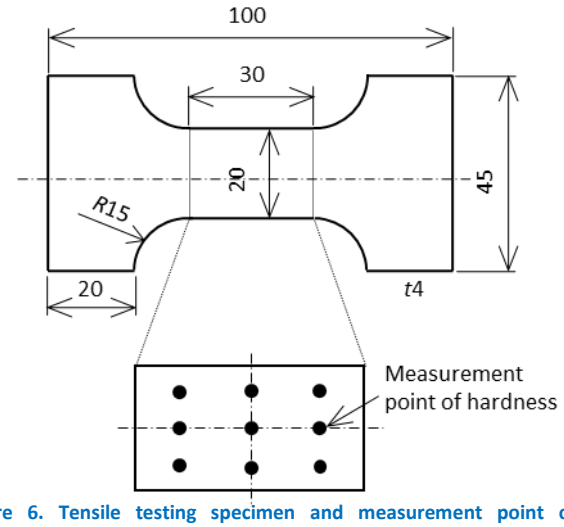

Figure 6. Tensile testing specimen and measurement point of hardness

the order of 150, 500, 800, and 2000 grit, and finished to a mirror surface. Next, nitric acid concentration of 5% with nital were etched for 30 seconds. The obtained corrosion surface was observed with an industrial microscope (Nikon, ECLIPSE L150) to examine its relationship with Vickers hardness.

3 RESULTS AND DISCUSSIONS

3.1 *X-ray CT analysis and simulation results for different injection speeds*

The internal porosities of X-ray CT images in a thickness of 16 mm with the second speed of injection are presented in Fig. 7. In the figure, the material is shown as the gray area and the void (where air bubbles exist) is shown as black specs or lines. Shrinkage porosities which grow in arch-like shapes can be observed grown in the injection speed of 2.0 m/s as shown in Fig. 7(a). On the other hand, many spherical porosities were observed in the injection speed of 5.0 m/s as shown in Fig. 7(b). The difference of porosity types was due to the fluid behavior and cooling rate when passing through the gate. A fast gate speed induces a spray flow. Therefore, the amount of air entrainment increases in a cavity [Cao 2019, Ibrahim 2020]. Similar phenomenon was caused in Fig. 7(b). In contrast, the shrinkage porosities with the injection speed of 2.0 m/s were distributed near the wall. We considered that the solidification near the wall surface occurs faster than the filled time. Moreover, the solidification shrinkage was spread due to poor pressure propagation [Iwata 2012].

Fig. 8 shows the porosity volume in relation with the second speed of injection. The figure compares the X-ray CT analysis and the simulation results. In the figure, the circular plot shows the X-ray CT analysis result, and the cross plot shows the simulation result. The color yellow shows the second injection speed 2.0 m/s, and green shows the second injection speed 5.0 m/s. In Fig. 9, the comparison between number of porosities with the second speed of injection for simulation and experimental results are shown. In the figure however, the rhombus plot shows the X-ray CT analysis result, and the cross plot shows the simulation result. The results shows that the porosity volume has increased as the injection speed increases. Therefore, the air entrainment in the cavity increased as the gate speed increases. However, the simulation and the X-ray CT analysis results were different more than 50%. In the injection speed of 2.0 m/s, the simulation result has lower porosity volume from 50% to 80% compared to the CT analysis. Furthermore, in the injection speed of 5.0 m/s, the simulation result has lower porosity volume, ranging from 70% to 90% compared to the CT analysis. It was considered that the reason why the porosity measurements for experimental and simulation were due to the difference in the definitions of a porosity. Within an actual casting, porosity exists in complex shape as shown in Fig. 10. In the Fig. 10(a), (b), and (c), a scale bar shows a length of 0.15 µm, 0.2 µm, and 0.3 µm, respectively. The actual porosity has unique form like back-to-back of two people as shown in Fig. 10(a), like a dinosaur as shown in Fig. 10(b), like a big head person as shown in Fig. 10(c). The complex porosity shapes obtained in X-ray CT analysis were produced in combination with air porosities and shrinkage porosities. That is, even if the number of porosities in experiment is less than the simulation result, the porosity volume in experiment is greater than the simulation result. On the contrary, a porosity in the simulation is defined as sphere. In addition, the simulation of the molten metal flow only considered the air entrainment. Hence, the shrinkage porosity volume was not evaluated. Some shrinkage porosities are those

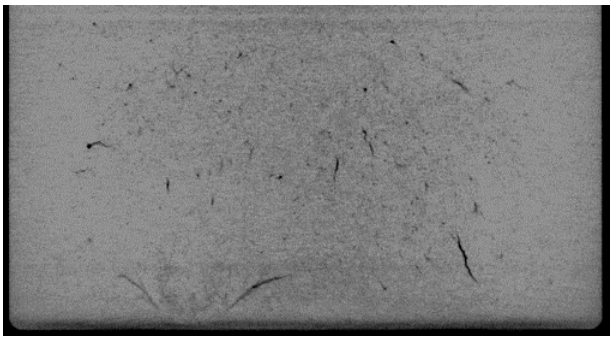

(a) Shrinkage porosities at the injection speed of 2.0 m/s

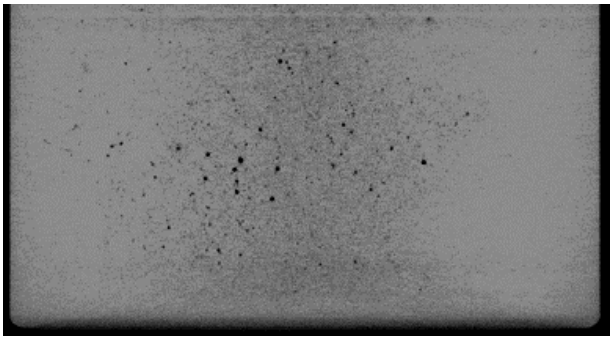

(b) Spherical porosities at the injection speed of 5.0 m/s

Figure 7. Porosity distribution in 16 mm thickness

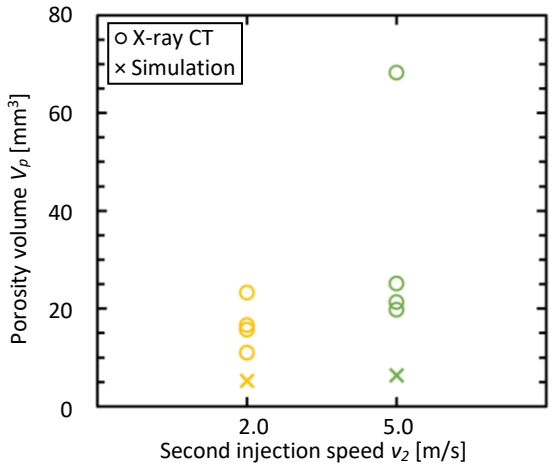

Figure 8. Relationship between second speed of injection and porosity volume

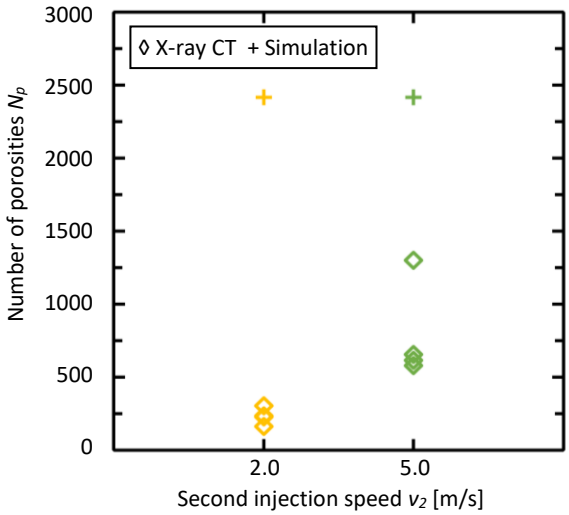

Figure 9. Relationship between second speed of injection and the number of porosities

having irregularly shaped with a larger volume than some porosities of air entrainment. Many shrinkage porosities were observed at the injection speed of 2.0 m/s. Therefore, it was considered that the porosity volume in the simulation had difference with the experiment. As such, it is important that the casting simulation consider the shrinkage porosity in the next stage.

3.2 Tensile strength and microstructure

Fig. 11 shows the tensile strength for the plate thickness of 4 mm with the second speed of injection. In the figure, the square yellow plot shows the second injection speed 2.0 m/s, and the square green plot shows the second injection speed 5.0 m/s. The tensile strength increased because of the increase of the injection speed. The tensile strength has low variability at the injection speed of 5.0 m/s. Fig. 12 shows the Vickers hardness (HV) for the plate thickness of 4 mm with the second speed of injection. The figure compares the step side and the flat side. In the figure, the rhombus orange plot shows the step side hardness, while the triangular blue plot shows the flat side hardness, and the bar shows a range of their scatter from a maximum to a minimum value. The Vickers hardness increases as the injection speed increases, and the difference of HV between the step side and the flat side decreases. The Vickers hardness at an injection speed of 2.0 m/s has a difference of about 4 HV between the step side and the flat side. On the other hand, the difference of the HV for the 5.0 m/s was less than 1 HV. These results were influenced by the morphology of the metal microstructure. Fig. 13 and 14 show the surface microstructure for the plate thickness of 4 mm. In the figures, the white area shows the primary phase α-Mg, and the black area shows the eutectic phase. The scale bar is 50 μm. The coarse primary phase α-Mg was present at the injection speed of 2.0 m/s as shown in Fig. 13(a) and 13(b). Although, it was observed that the primary phase α-Mg in the injection speed of 5.0 m/s as shown in Fig. 14(a) and 14(b) was finer than the one of that 2.0 m/s speed. The quick injection allowed the high-temperature molten metal to spread quickly into the cavity. Then, the eutectic phases quickly formed because of shorter filling time and cooling time. Therefore, the growth of the primary phase α-Mg was suppressed. As a result, a stronger and denser microstructure was successfully obtained. On the other hand, if the injection speed is slower, the α-Mg growth progresses because of the increased cooling time. The large number of dendritic primary phases were observed on the flat side in the injection speed of 2.0 m/s as shown in Fig. 13(b). It was considered that the tensile strength and Vickers hardness were greatly reduced by these coarse primary phases. Moreover, the strong flow via the gate on the flat side delayed the solidification. Therefore, the primary phase on the flat side was coarsened.

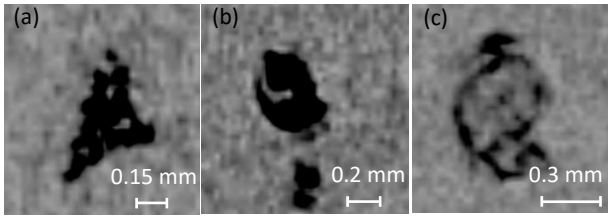

Figure 10. Complex porosity shapes with a combination air porosities and shrinkage porosities: (a) like back-to-back, (b) like a dinosaur, (c) like a big head

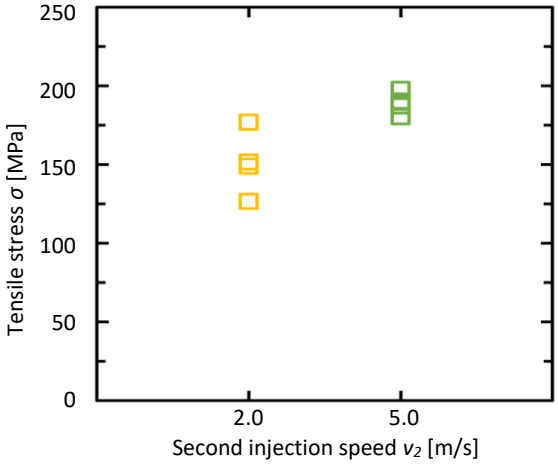

Figure 11. Relationship between casting condition and tensile stress in 4mm

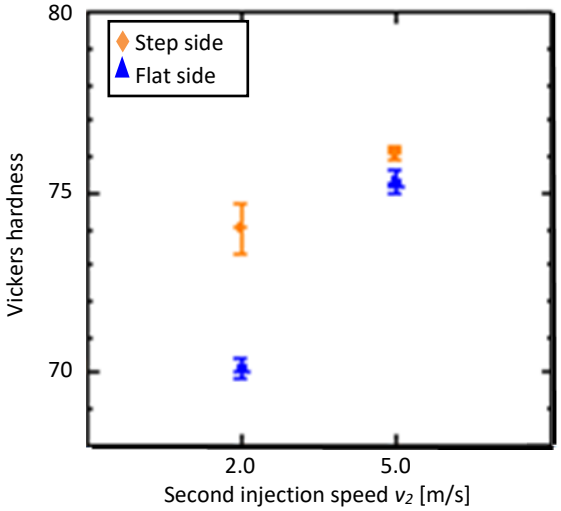

Figure 12. Relationship between casting condition and Vickers hardness in 4 mm

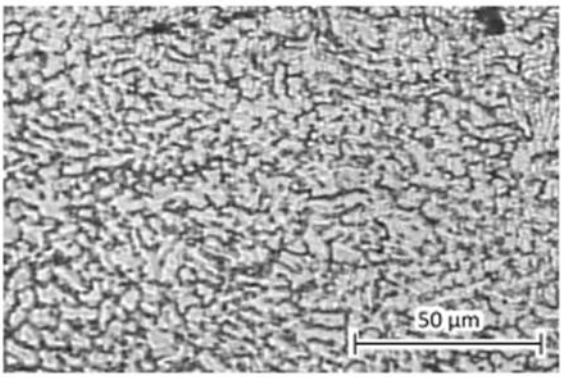

(a) Microstructure of step side

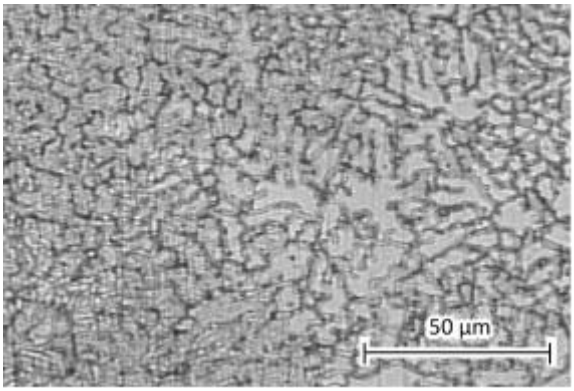

(b) Microstructure of flat side

Figure 13. Surface microstructure in the injection speed of 2.0 m/s on 4mm thickness

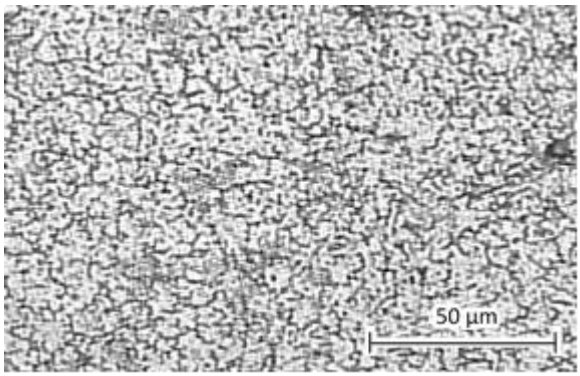

(a) Microstructure of step side

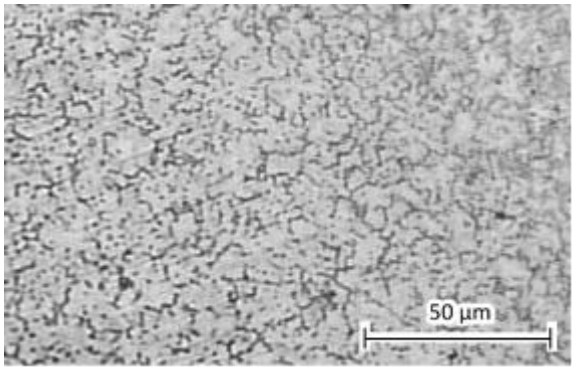

(b) Microstructure of flat side

Figure 14. Surface microstructure in the injection speed of 5.0 m/s on 4mm thickness

4 CONCLUSIONS

In this study, in order to clarify the unknown physical properties of the Mg-Al-Th-RE alloy, the relationship between casting conditions and internal porosities and the mechanical properties exerted by the solidification microstructure were investigated. The X-ray CT analysis and simulation results showed that the porosity volume has increased as the injection speed increases. However, the simulation and the X-ray CT analysis results were different more than 50% because of the difference in the definitions of a porosity. There were many shrinkage porosities like an arch grown in the injection speed of 2.0 m/s. On the other hand, many spherical porosities were observed in the injection speed of 5.0 m/s. The difference of porosity types was due to the fluid behavior and cooling rate when passing through the gate. The higher injection speed also affected the increase of the material strength and hardness, and the reduce of the variability. This result was attributed the morphology of the metal microstructure. It was observed that the primary phase α-Mg in the injection speed of 5.0 m/s was finer than the one of that 2.0 m/s speed. The eutectic phases quickly formed because of shorter the filled time and the cooled time. Therefore, the growth of the primary phase α-Mg was suppressed. On the other hand, if the injection speed is slower, the dendritic primary phase α-Mg growth progresses because of the increase of cooling time. It was considered that the tensile strength and Vickers hardness were greatly reduced by these coarse primary phases.

ACKNOWLEDGMENTS

This research was partially funded by Kyokuto Die-Casting Co., Ltd., while the X-ray CT measurements conducted in this work was supported by Tokai University Imaging Research Center. This research was also partially supported by Universiti Malaysia Sarawak.

REFERENCES

[Beals 2004] Beals, R., et al. Fundamental Research Needs for the Magnesium Powertrain Cast Components (MPCC) Project. In: A. A. Luo, ed. Proceedings of the Magnesium Technology 2004, Warrendale, January, 2004, Pennsylvania: The Minerals, Metals & Materials Society, pp 11-17.

[Cao 2019] Cao, H., et al. Direct Observation of Filling Process and Porosity Prediction in High Pressure Die Casting. Materials, April 2019, Vol. 12, Issue 7, pp 1-19. ISSN 1996-1944

[Cleary 2014] Cleary, P. W., et al. Flow analysis and validation of numerical modelling for a thin walled high pressure die casting using SPH. Computational Particle Mechanics, May 2014, Vol. 1, Issue 3, pp 229-243. ISSN 2196-4386

[Ebel-Wolf 2008] Ebel-Wolf, B., et al. Influence of elevated temperatures on the cyclic deformation behaviour of the magnesium die-cast alloys AZ91D and MRI230D. Materials Science and Engineering: A, July 2008, Vol. 486, Issues 1-2, pp 634-640. ISSN 0921-5093

[Fukatsu 2021] Fukatsu, T., et al. Development of mass-production die-casting technology for heat-resistant, high-strength magnesium alloy. In: Society of Automotive Engineers of Japan, Inc. ed. 2021 JSAE Annual Congress (Spring), Online, May, 2021, Online: Society of Automotive Engineers of Japan, Inc., p 1.

[Gaspar 2016] Gaspar, S. and Pasko, J. The Research of the Fracture Process and Analysis of the Foundry Errors of Die Castings from Hypoeutectic Silumin. MM Science Journal, November 2016, pp 1265-1268. ISSN 1803-1269

[Gaspar 2019] Gaspar, S. and Pasko, J. Plunger Pressing Speed Link the Main Factor Influencing of the Mechanical Properties of Die Casting. MM Science Journal, December 2019, pp 3490-3493. ISSN 1803-1269

[Ibrahim 2017] Ibrahim, M. D., et al. Effect of mold designs on molten metal behaviour in high-pressure die casting. Journal of Physics: Conference Series, 2017, Vol. 822, No. 012029, pp 1-6. ISSN 1742-6596

[Ibrahim 2018] Ibrahim, M. D., et al. Characteristics of Modified Spiral Thrust Bearing through Geometries and Dimension Modifications. Tribology Online, December 2018, Vol. 13, No. 6, pp 334-339. ISSN 1881-2198

[Ibrahim 2020] Ibrahim, M. D., et al. Numerical and Experimental Analysis on Runner and Gate Positioning for Magnesium Alloy Die-Casted Test Piece. Materials Science Forum, January 2020, Vol. 975, pp 242-247. ISSN 1662-9752

[Iwata 2012] Iwata, Y., et al. Compression Behavior of Entrapped Gas in High Pressure Diecasting. Materials Transactions, March 2012, Vol. 53, Issue 3, pp 483-488. ISSN 1347-5320

[Kikuchi 2019] Kikuchi, H., et al. Evaluation of Lubrication Performance of Foil Bearings with New Texturing. Tribology Online, December 2019, Vol. 14, No. 5, pp 339-344. ISSN 1881-2198

[Kuriyama 2012] Kuriyama, Y. and Yano, K. Multi-Subcenters Solution Search Algorithm for CFD Optimization Problems and Its Application to Die Casting. Materials Transactions, February 2012, Vol. 53, Issue 2, pp 367-373. ISSN 1347-5320

[Mizutani 2019] Mizutani, M., et al. Features and Vehicle Application of Heat Resistant Die Cast Magnesium Alloy. SEI

Technical Review. April 2019, No. 88, pp. 116-121. Osaka: Sumitomo Electric Industries, Ltd., 2019.

[Mondal 2010] Mondal, A. K., et al. Interrupted creep behaviour of Mg alloys developed for powertrain applications. Materials Science and Engineering A, April 2010, Vol. 527, Issue 9, pp 2289-2296. ISSN 0921-5093

[Moscovitch 2007] Moscovitch, N., et al. Design Guidelines for Components Die Cast in Creep-Resistant Magnesium Alloys MRI153M and MRI230D. SAE Technical Paper, April, 2007: SAE International in United States, pp 1-8. ISSN 0148-7191

[Niida 2020] Niida, A. and Maeda, Y. Observation of Air Entrapment during Mold Filling of Die Casting Using Water Model Experiment for Mold Filling Simulation. Materials Transactions, July 2020, Vol. 61, Issue 7, pp 1364-1368. ISSN 1347-5320

[Rimar 2016] Rimar, M., et al. Dependence of Hardness of Continues Die-casting Products on Fe Content. MM Science Journal, November 2016, pp 1201-1204. ISSN 1803-1269

[Roslan 2018] Roslan, L. B., et al. Flow Simulation and Experiment for preventing Defects in Die Casting. In: Japan Die Casting Association ed. 2018 Japan Die Casting Congress Transactions, Yokohama, November, 2018, Japan: Japan Die Casting Association, pp 119-122 (in Japanese).

[Sun 2020] Sun, Z., et al. Microstructure, Tensile Properties and Fracture Behavior of HPDC Magnesium Alloy AZ91. International Journal of Materials, Mechanics and Manufacturing, April 2020, Vol. 8, No. 2, pp 50-56. ISSN 1793-8198

[Yanagihara 2015] Yanagihara, E., et al. Precipitation Structure of Al-10 mass%Si-0.3 mass%Mg Alloy Produced by High Pressure Die Casting and Permanent Mold Casting with T5 Treatment. Materials Transactions, July 2015, Vol. 56, Issue 7, pp 1112-1119. ISSN 1347-5320

CONTACTS:

Yuki Kashiwabara, M.Eng.
Tokai University, Graduate School of Science and Technology, Course of Science and Technology
4-1-1 Kitakaname, Hiratsuka, Kanagawa, 259-1292, JAPAN
Tel.: +81 463 58 1211, e-mail: y.kashiwabara.snmlab@hope.tokai-u.jp

Assoc. Prof. Ir. Dr. Mohd Danial Ibrahim, Dr.Eng.
Universiti Malaysia Sarawak, Faculty of Engineering, Department of Mechanical and Manufacturing Engineering
Jalan Datuk Mohammad Musa, 94300 Kota Samarahan, Sarawak, MALAYSIA
Tel.: +6 082 58 1000, e-mail: imdanial@unimas.my

Sen. Lect. Dr. Lidyana Binti Roslan, Ph.D.
Universiti Malaysia Sarawak, Faculty of Engineering, Department of Mechanical and Manufacturing Engineering
Jalan Datuk Mohammad Musa, 94300 Kota Samarahan, Sarawak, MALAYSIA
Tel.: +6 082 58 1000, e-mail: rlidyana@unimas.my

Hitoshi Watanabe, M.Eng.
Kyokuto Die-Casting Co., Ltd.
57 Mukohara, Yamakita, Ashigarakami, Kanagawa, 258-0111, JAPAN

Assoc. Prof. Dr. Yuta Sunami, Dr.Eng.
Tokai University, Department of Mechanical Engineering
4-1-1 Kitakaname, Hiratsuka, Kanagawa, 259-1292, JAPAN
Tel.: +81 463 58 1211, e-mail: sunami@tokai-u.jp